Photolysis of frozen iodate salts as a source of active iodine in the polar environment

Óscar Galvez[1], M. Teresa Baeza-Romero[2], Mikel Sanz[3] and Alfonso Saiz-Lopez[4]

[1]{Departamento de Física Molecular, Instituto de Estructura de la Materia, IEM-CSIC, 28006 Madrid, Spain}. Now at {Departamento de Física Interdisciplinar, Facultad de Ciencias, Universidad Nacional de Educación a Distancia, 28040, Madrid}.

[2]{Escuela de Ingeniería Industrial, Universidad de Castilla-La Mancha, 45071, Toledo, Spain}

[3] {Escuela de Ingeniería Industrial, Universidad de Castilla-La Mancha, 45071, Toledo, Spain}. Now at {Institute of Physical Chemistry Rocasolano, CSIC, 28006 Madrid, Spain}

[4] {Department of Atmospheric Chemistry and Climate, Institute of Physical Chemistry Rocasolano, CSIC, 28006 Madrid, Spain}

Correspondence to: O. Gálvez (oscar.galvez@csic.es) (oscar.galvez@ccia.uned.es)

Abstract

Reactive halogens play a key role in the oxidation capacity of the polar troposphere. However, sources and mechanisms, particularly those involving active iodine, are still poorly understood. In this paper, the photolysis of an atmospherically relevant frozen iodate salt has been experimentally studied using infrared (IR) spectroscopy. The samples were generated at low temperatures in the presence of different amounts of water. The IR spectra have confirmed that under near-UV/Vis radiation, iodate is efficiently photolyzed. The integrated IR absorption coefficient of the iodate anion on the band at 750 cm^{-1} has been measured to be A= 9.8 ± 0.5 x 10^{-17}cm $molec^{-1}$. The photolysis rate of the ammonium iodate salt was measured by monitoring the decay of ammonium or iodate IR bands (1430 and 750 cm^{-1} respectively) in the presence of a solar simulator. The absorption cross section of the liquid

solutions of ammonium iodate at wavelengths relevant for the troposphere (250 to 400 nm) has been obtained, and used to estimate the photolytic quantum yield for the frozen salt. Finally, using an atmospheric model, constrained with the experimental data, we suggest that the photolysis of iodate in frozen salt can potentially provide a pathway for the release of active iodine to the polar atmosphere.

1 Introduction

Atmospheric iodine compounds are present in the marine and polar boundary layers (Saiz-Lopez et al., 2012), where they play a relevant role in catalytic ozone destruction (Saiz-Lopez et al., 2007b) (Read et al., 2008), and they could also be involved in new particle formation in the polar environment (Allan et al., 2015;Roscoe et al., 2015). Moreover, in the polar atmosphere, iodine has also been suggested as one of the possible sinks of gaseous elemental mercury (Calvert and Lindberg, 2004;Saiz-Lopez et al., 2008).

Although the concentration of atmospheric iodine is highly variable at different regions, ground- (Frieß et al., 2001) (Saiz-Lopez et al., 2007b) (Atkinson et al., 2012) and satellite-based instrumentation (Saiz-Lopez et al., 2007a;Schönhardt et al., 2008) measurements have confirmed remarkably high concentrations (up to 20 pptv) of IO in coastal Antarctica. Nevertheless, the sources and mechanisms of iodine emissions from ice remain poorly understood (Saiz-Lopez et al., 2015;Kim et al., 2016).

Apart from observations of gaseous iodine species, different studies have conducted analysis of the iodine fraction in rainwater (Laniewski et al., 1999) and aerosols (Baker et al., 2000). In all of them, iodine concentrations are considerably enriched over seawater, and an appreciable fraction of soluble iodine species like I^- and IO_3^- is observed, although the mechanism determining the I^-/IO_3^- ratio is still unclear. Thus, for example since IO_3^- has been considered an inert inorganic iodine species, and therefore a sink molecule in the atmospheric iodine cycle, model calculations (Pechtl et al., 2006) suggest that IO_3^- should accumulate in marine aerosol. However, several field campaigns (Baker, 2004;Gilfedder et al., 2008) have revealed that the iodide/iodate ratio is rather variable in aerosol, showing significant I^- concentration.

A recent study has suggested that IO_3^- anions show a substantial reactivity in frozen solutions under near-UV/Visible light irradiation (Spolaor et al., 2013). During the irradiation of IO_3^-

frozen solutions reactive gaseous iodine species were produced and converted to iodine oxide particles (IOP) for detection. Inspired by these results, we have further studied the photo-stability of iodate frozen salts to assess its potential role in iodine emissions to the polar atmosphere. In this work, we have determined the absorption cross section of the NH_4IO_3 solution, which has been used to estimate for the first time the absorption cross section and quantum yield of frozen ammonium iodate solutions at wavelengths relevant for the troposphere, from 250 to 400 nm. The product of these two quantities gives us the efficiency of the photolytic process, but these values should be taken as a lower limit that needs to be explored in further detail in future laboratory work. This information has been incorporated into an atmospheric model to assess the potential of iodate photolysis to release reactive iodine to the Antarctic boundary layer during springtime.

2 Experimental methods

For the study of the photolysis of iodate salts, we have tested several iodated compounds. Firstly, the photolysis of frozen solutions of KIO_3 was studied, and significant photolysis was observed (for more details see supplementary section). However, due to the overlapping of the IO_3^- IR band with water absorption, we studied NH_4IO_3 since:

(i) As mentioned above, it was not possible to monitor iodate signal in the presence of high concentration of water since the infrared iodate band overlaps with water absorptions. The fact that the chosen salt has a cation like NH_4^+ that presents a band with no interference (and that it is consumed in a 1:1 ratio with iodate, see supplementary section) allowed us to measure the photolysis of iodate indirectly as described below.

(ii) As far as we know, there is no information in the literature of the integrated value of the IR absorption coefficient of iodate band, and in consequence, it was not possible to directly quantify the amount of iodate in the samples. One of the possibilities to solve this problem is to use an iodate salt for which the integrated absorption coefficient of the IR band of the counter-ion was known, like ammonium iodate. This was the procedure that we have followed, and more details of these calculations are given in the next section.

(iii) Moreover, ammonium iodate is expected to be an abundant iodate salt in the atmosphere, since ammonium concentrations are high in some environments, and it could be deposited into the ice as large fluxes of iodinated compounds have been observed during glacial period

(Spolaor et al., 2013), and the presence of ammonium ions in ice samples is also expected. Moreover, ammonium and iodinated compounds have been detected at the same time in melting Artic sea ice, implying that this salt could be atmospherically relevant (Assmy et al., 2013). Note however, that other salts such as $NaIO_3$ or KIO_3 would be representative of polar environments too, and further experiments using these compounds should be addressed in the future.

Solid samples containing iodate anions were produced through the sudden freezing of droplets of aqueous solutions of NH_4IO_3 on a cold Si substrate located inside a vacuum chamber. A detailed description of the experimental setup can be found elsewhere (Maté et al., 2009;Gálvez et al., 2010), and only a brief description of the most relevant aspects for the present experiments is given here. The solid substrate is mounted in a Cu block in contact with a liquid nitrogen Dewar. The substrate temperature can be controlled with 1 K accuracy between 90 K and 300 K. The vacuum chamber, which is coupled to a Vertex70 Bruker FTIR spectrometer through a purged pathway, is evacuated with a turbomolecular pump to a background pressure of $\sim 10^{-8}$ mbar. Transmission spectra of the samples were recorded, with 2 cm^{-1} resolution, using an MCT (Mercury Cadmium Telluride) detector refrigerated with liquid nitrogen. Liquid solution droplets from a room temperature pulsed valve (General Valve, series 9), usually employed for the generation of free jets and molecular beams (Abad et al., 1995), were made to impinge on the cold Si substrate placed at ~15-20 mm. When a desired amount of sample is on the substrate, this can be rotated to record the IR spectra, or to be processed by simulated Solar light. A scheme of the experimental setup is shown in Fig. 1. Solar irradiance was simulated by a 1000 W LOT® Xenon Arc lamp that radiate between around 250 nm to 2.5 μm, although an important fraction of the output is given below 900 nm according to the supplier of this lamp, where a fairly constant spectral irradiance is obtained between 300 to 900 nm. Power light received on the substrate is measured by a portable meter Thermal Detector, model 407A by Spectra-Physics, which operates in a wavelength range from 250 nm to 11 μm without significant sensitivity variations (less than 3 %).

UV-Vis spectra of the studied salts were obtained in water solution at different concentrations using both an UV-Visible Uvikon spectrophotometer 930 from Kontron Instruments and a double-beam spectrophotometer (Shimadzu UV-3600), equipped with quartz cuvettes of 10 mm size. The spectra resolution was fixed at 0.5 nm, from 190 to 500 nm.

In all experiments, a pulsed valve was filled with a solution 0.1 M of ammonium iodate (Across Organics, for analysis). A slight He overpressure behind the liquid solution filling the valve improved the performance. This generation procedure does not lead to an uniform film, and the thickness of the ice samples, which typically range from ~0.1 to 1 μm (Mate et al., 2012), can vary among different experiments. Solid samples generated by this technique contain compact ices structures in a hyperquenched glassy water morphology (Mayer, 1985), in which the water molecules retain their amorphous liquid structure, and where ions are solvated by water molecules instead of being segregated in the ice (Mate et al., 2012). When the temperature of the substrate is below that of water sublimation (around 170 K), the ice mixture concentration is somewhat comparable to the liquid solution (0.1 M), and the infrared spectra of these ices are largely dominated by water absorptions. In these cases, water bands hide the IR features of the salt, and prevent monitoring its evolution during irradiation. For this reason, most samples were slowly warmed above water sublimation to achieve a lower water concentration to avoid such interference. Nevertheless, some samples were also reserved in their original diluted salt proportion to explore the effect of this variable. We refer to the samples that have suffered this process as *hyperquenched (HQ) samples*, as their morphology is provided by the hyperquenching technique. However, in other experiments, samples deposited by hyperquenching are annealed to high temperature (up to 240 K for around 10 minutes) to dry them completely, and then, after cold down to a selected low temperature (e.g. 100 or 140 K), a controlled water vapour flux is added to be adsorbed onto the dried salt, condensing on the sample. With this procedure, solid samples present a different morphology since water molecules are deposited uniformly on the salt surface resulting in a more porous structure. In addition, when the condensation of water occurs at 100 K, a homogeneous film of low-density amorphous water ice is deposited on top of the salt, but at deposition temperature of ca. 140 K or above, the ice film has crystal cubic ice structure (Mate et al., 2012). When this technique is used and water is added from vapour phase, we refer to these samples as *Vapour deposited (Vap) samples*.

Initially, deposition at low temperature (< 120 K) leads to amorphous ices samples, which show high specific surface areas (SSA) (Mate et al., 2012), around 100 times higher, or even more, than typical atmospheric ice samples. However, when temperature is increased at 140 K, amorphous samples are irreversibly transformed to cubic crystal ice, leading to a reduction of the SSA by a factor of 100 or even higher (Ocampo and Klinger, 1982), which are common values of freshly atmospheric ice samples. It is worth noting that amorphous solid water

(ASW) has been recently chosen as a model for the disordered interstitial air-ice interface within snowpack (Marcotte et al., 2015).

Due to the requirements of the experimental setup, the ratio of NH_4IO_3:H_2O in the samples is considerable much higher than for environmental ices, however, some more diluted samples were also studied to assess this effect on the photolysis process.

To summarize the procedure to generate the samples: they were firstly generated by HQ deposition at 100, 140, 160, 200, 260 or 298 K, after deposition at those temperatures, three different processes were carried out: (i) the samples at the deposition temperature were just irradiated, (ii) samples deposited at low temperatures were firstly annealed to around 170 K for some minutes to eliminate part of the water, then cool down to a certain low temperature (from 100 to 140 K) and then irradiated, (iii) or samples were annealing until to 240 K for around ten minutes to dry them completely, then they are cooled down at a selected low temperature at which a certain amount of water from vapour phase was deposited, and finally irradiated. A complete list of all the samples and deposition conditions (and the resulting rate constants of the photolysis process) is included in Table S1 in the supplementary material.

2.1 Determination of the concentration of the different species in the samples

Column densities of water, NH_4^+ and IO_3^- ions in the ice mixtures were calculated via the Lambert–Beer equation, using the integrated values of the infrared absorption bands, and the corresponding integrated absorption coefficients, *A*. The bands chosen for this purpose were the ν_2 and $\nu_2+\nu_R$ bands of water around 1650 and 2220 cm^{-1}, respectively, the ν_4 band of NH_4^+ around 1430 cm^{-1}, and the ν_3 band of IO_3^- at approx. 740 cm^{-1}. For water band intensity, we have used the values reported by Mastrapa *et al*. (Mastrapa et al., 2009) for an amorphous or crystalline (cubic) phase at 100 K. For *Vap* samples at 100 K the values of amorphous ice used are: $A(H_2O)_{amorphous}$ = 1.6 x 10^{-17} and 9.8 x 10^{-18} cm $molec^{-1}$, while for *Vap* samples at 140 K or *HQ* samples (when water was annealed at higher temperatures) the integrated absorption coefficients of cubic ice are more representative: $A(H_2O)_{cubic}$ = 1.8 x 10^{-17} and 1.1 x 10^{-17} cm $molec^{-1}$, for 1650 and 2220 cm^{-1} bands. In the case of NH_4^+, different values of the absorption coefficient have been reported in the literature, ranging from 2.5 to 4.4 x 10^{-17} cm $molec^{-1}$ (Maté et al., 2009) (Schutte and Khanna, 2003). Due to these discrepancies, we have selected a suitable value of 4.0 x 10^{-17} cm $molec^{-1}$, close to that given by Schutte & Khanna (Schutte and Khanna, 2003) for solid samples, which are more representative of our case. For

iodate, we are not aware of previous data of *A* values in the IR region, so we have determined it in this paper. In this case, we have estimated this value for pure ammonium iodate samples, based on that previously given for NH_4^+, obtaining a mean integrated absorption coefficients $A(IO_3^-) = 9.8 \pm 0.5 \times 10^{-17}$ cm molec^{-1} for the band centred at 750 cm^{-1} (details are shown in the supplementary material).

2.2 Calculation of spectral irradiance received by the samples

We assumed that the observed photolysis of ammonium iodate samples should be mainly due to the highest frequency photons (below 400 nm) emitted by the Solar lamp. The reason is that IO_3^- in aqueous media absorbs light only in the UV range (Awtrey and Connick, 1951), at wavelengths below 270 nm, which is also in agreement with our near UV-Vis spectra of iodate salts (see Fig. 2). For this reason, it is important to delimit the blue-cut-off of the irradiation received by the samples, which is determined by the glass window of the vacuum chamber (see Fig. 1). In consequence, the UV-Vis spectrum of the glass window was recorded to define the transparent interval of frequencies, especially the UV cut-off, see Fig. 2. Taking into account this spectrum, and in combination with that provided by the lamp manufacturer for the spectral irradiance of the lamp at 0.5 m, we can estimate that only 6.3 % of the total lamp power received by the substrate allocated inside the vacuum chamber is due to light of wavelengths below 400 nm (see supplementary section for more details). Consequently, since our thermopile covers the whole range of frequencies without significant variations, and taking into account that the average reading in the thermopile along the experiments was around 1.5 W cm^{-2} (which was regularly monitored during the experiments), we can estimate that the substrate was irradiated with an average light power of 0.095 W cm^{-2}, within the wavelength range of 250 to 400 nm.

In order to illustrate whether this irradiance power is characteristic of environmental conditions, it could be compared with the average irradiance (also below 400 nm) received at the Earth´s surface which has been estimated around 0.01 W cm^{-2} (see supplementary section for more details), which result in around 9 times lower irradiance than that received by the samples in our experiments. Nevertheless, we should take into account several additional factors. For instance, our silica substrate is highly reflective to visible light, therefore since the irradiation occurs perpendicularly to the substrate (see Fig. 1), probably our samples received double flux (incident and reflected) than that above calculated. This factor sets our calculated irradiance power as a lower limit. On the contrary, note that due to our

experimental procedure, samples are not homogeneously distributed on the substrate, and thus the photon flux impacting on the samples was, to a certain degree, lower. These considerations are further explored in the following section.

Note that, due to the limitations mentioned above and the use of the thermopile for the determination of the photon flux, it presents limitations and uncertainties (thermopile is practically insensible to photon frequency), and other methodologies (as for example the use of chemical actiometers) could be more adequate to quantify this parameter.

3 Results and Discussions

3.1 Laboratory experiments

Fig. 3 shows IR spectra of different samples of solid ammonium iodate salt (with a small water proportion) at 200 and 100 K including those of 4 and 2:1 H_2O/NH_4IO_3 ice mixtures deposited at 100 K obtained by the hyperquenching (*HQ*) technique or via vapour deposited (*Vap*) H_2O, respectively. Table 1 displays the positions of IR bands of NH_4IO_3. These IR spectra are as well shown in Fig. 3. All experiments and conditions are summarized in Table S1 in supplementary section. Sharper and more defined bands of NH_4^+ and IO_3^- appear in spectra at 100 K, showing also a slight displacement, which are typical effects when temperature is decreased (Gálvez et al., 2009). When water is present, IO_3^- bands undergo a small blue-shift, which can be related to the overlap with the ν_R libration water mode at ca. 800 cm^{-1}. Moreover, some differences in the water bands become visible on the spectra of the mixtures, arising from the solid structure of water ice. In the *HQ* sample shown in Fig. 3, due to the crystallization processes undergone during the annealing, the IR spectrum show typical water bands of a cubic phase. In the case of *Vap* samples, water ices present a low-density amorphous structure, which corresponds to deposition at 100 K, showing broader bands in the IR spectrum.

After generation, all samples were irradiated during 3 to 5 hours by a 1000 W Xenon Arc lamp. In all cases NH_4^+ and IO_3^- IR bands diminish during irradiation process, which is especially evident when 1430 and 745 cm^{-1} bands are monitored. The dependence of the reduction of these two bands have been analysed in detail. In Fig. 4, we show the plot of $\ln(Int(IO_3^-)_t/Int(IO_3^-)_0$ vs $\ln(Int(NH_4^+)_t/Int(NH_4^+)_0$ for the samples. The data of the different linear fittings are collected in Table 2. Note that this correlation is more difficult to examine

in the case of IO_3^-/H_2O ratio higher than 1, due to: i) the overlap of water and IO_3^- bands, ii) and the changes that integrated absorption coefficients of NH_4^+ and IO_3^- infrared bands could undergo in the presence of water, due to the intermolecular hydrogen bond formed in the hydration process. Therefore, when this analysis was carried out for ice mixtures with higher water proportions, it yields values that could not be adjusted to a line or the slopes obtained by the best linear fitting were far from typical values, revealing the problems highlighted above. Nevertheless, and taking into account these considerations, the linear fittings present a R^2 value usually higher than 0.99. According to the Table 2, we can observe that the analysis for samples irradiated at low temperatures (from 100 to 200 K) yield similar slopes, showing a mean value of 0.72 ± 0.05, or a mean slope value of 0.758 when all the points are included in the linear fitting (see Fig. 4). However, for samples irradiated at temperatures above 200 K (at 253 or 298 K), this analysis yields higher slope values, with a mean slope of 1.01 ± 0.07 (or 0.973 when the points for all the experiments are included in the same linear fitting, see Fig. 4), which could be considered in fact as 1. These different results could be explained by the formation of a volatile I_xO_y product during the photolysis of IO_3^-, which could be retained in the matrix at temperatures below 200 K. This product typically would show IR absorptions around 740 cm^{-1} (corresponding to the stretching of I-O bond, see Maier and Bothur (Maier and Bothur, 1997)), and this fact would give a lower rate of diminishing for the 740 cm^{-1} band intensity with respect to that at 1400 cm^{-1} (ascribed only to NH_4^+). At higher temperatures, this product could scape to the gas phase resulting in a 1:1 ratio in the decay of both bands. According to this result, it seems appropriate to assume a 1:1 relationship between NH_4^+ loss and IO_3^- loss in the photolysis of these ices at atmospheric relevant temperatures.

It is important to note that there was not evolution of the IR spectra of the samples observed in dark conditions (this fact was checked many times along the experimental measurements).

Typical UV-Vis spectra of common ammonium salts (i.e. NH_4Cl) do not display significant absorption bands in the near-UV and visible regions (see Fig. 2), and, to the best of our knowledge, no literature exists on the photolysis of these species. Based on this, the photolysis of ammonium ions is not expected to occur in this spectral range. Therefore, reduction of the IR ammonium bands should be caused by a fast reaction with "reacting" species produced by photolysis of frozen iodate during the irradiation process: HOI, IO and I_2 (Spolaor et al., 2013), or OIO (Klaning et al., 1981), or other reacting species (e.g.: oxygen atoms or anions, see above). It was previously observed that iodine reacts with ammonia in

aqueous solution (McAlpine, 1952), and consequently, we expected that any of these iodinated compounds obtained in the photolytic process, which could be even more reactive than I_2, could themselves react very fast with NH_4^+.

In addition to those changes at the 1430 and 740 cm^{-1} bands, other changes are evident in the IR spectra, revealing that not only ammonium and iodate ions are consumed, but also new products are formed (Table S1). These changes are more evident for the low-temperature experiments, around 100 K, since volatile products formed during the photolysis can also be retained on the substrate. Fig. 5 shows an example of a pure solid NH_4IO_3 salt deposited at 100 K and irradiated at that temperature. Dotted lines indicate bands that undergo clear changes during photolysis. Stretching NH_4^+ bands (around 3000 cm^{-1}) decrease with irradiation, although an increase of water band intensities, more evident in the peak around 3360 cm^{-1}, also occurs, probably due to the residual water background always present in the chamber (note that this effect only occurs at temperatures below 150 K). Two new peaks emerge during photolysis, around 2227 and 1300 cm^{-1}. To explain these bands, one possibility could be the formation of N_2O molecules that present infrared signal around 2200 cm^{-1}. The band around 1300 cm^{-1} can also be caused by N-O stretching vibration, which can arise from the reaction of O* species with ammonium. However, bands around 2227 cm^{-1} could belong to infrared absorptions of C-O stretching modes too. Slight carbon contamination mainly by CO_2 molecules are usually found in this type of experiments (Mate et al., 2014). Nevertheless, all these assignments should be considered as speculative.

The mechanism of iodate photolysis is largely unknown. In the study of Spolaor *et al.* (Spolaor et al., 2013), during the irradiation of IO_3^- frozen solutions, reactive gaseous iodine species were produced and converted to iodine oxide particles (IOP) for detection. In consequence, we suggest that probably the first step in the photolysis could be the formation of these active species. Mezyk and Elliot (Mezyk and Elliot, 1994) suggested the formation of IO_2 in the radiolysis of iodate solutions, and this species could also be formed in the photolysis of the ice mixtures, and after being transformed to OIO and reacts itself to form particles. The fact that the rate of decay of NH_4^+ and IO_3^- follows a ratio 1:1 suggests that this active species or one of its co-products reacts very fast with NH_4^+. In McAlpine´s work (McAlpine, 1952), it was proposed that some actives species of iodine like I_2, HIO can react with ammonia forming species like NH_2I, and perhaps eventually NI_3. Our experiment cannot

conclude about the exact mechanism, but it can confirm that NH_4^+ is consumed at the same rate that IO_3^-.

However, independently of the photolysis mechanism, the photolytic rate constant, *J* value, for the iodate ion can be calculated according to equation E1:

$$-\frac{d[IO_3^-]}{dt} = J[IO_3^-] \quad \text{(E1)}$$

The concentration of the iodate ion can be monitored by integration of the infrared band intensity at ca. 740 cm^{-1}, that, as shown in Fig. 4, could also be equivalent to monitor the NH_4^+ band at 1430 cm^{-1}:

$$-\frac{d[IO_3^-]}{dt} = J[IO_3^-] \quad \ll=\gg \quad -\frac{d[NH_4^+]}{dt} = J[NH_4^+] \quad \text{(E2)}$$

integrating E2 and considering that concentration is proportional to IR band intensity:

$$\ln(I_t) = \ln(I_0) - Jt \quad \text{(E3)}$$

where I_t and I_0 are the intensity of the band of NH_4^+ (or IO_3^-) at time *t* and zero, respectively.

According to E3, a representation of the natural logarithm of the integrated band intensities of NH_4^+ or IO_3^- signals versus time of photolysis will give us the *J* value, as the slope of the line of the best linear fit. This calculation has been done for all deposited samples at different temperatures and water concentrations (Table S1). Integration limits of the bands differ among the different samples, since the baseline of the spectra is rather sensitive to the generation process and morphologies of the ices mixtures. For this reason, the integration limits of the bands were adjusted for each sample in order to minimize the errors. The calculated mean value for all experiments (at the average light power calculated above) is $J = (4\pm2) \times 10^{-5}$ s^{-1} (see supplementary section for more details). Significant differences in the *J* values have not been observed among the samples prepared at different conditions, i.e. *Vap* or *HQ* deposition of water, different water ice structure (amorphous or cubic), different temperatures of generation and irradiation (from 100 to 298 K) or different amount of water in the mixtures. This suggests that the photolysis process does not notably depend on ice morphology, or even on the amorphous or crystalline structure, at least in the range of studied samples.

The photolysis rate can be also estimated according to E4:

$$J = \int_{\lambda_1}^{\lambda_2} F(\lambda)\sigma(\lambda)\phi(\lambda)d\lambda \quad \text{(E4)}$$

where $F(\lambda)$ is the radiative flux, $\sigma(\lambda)$ is the absorption cross section and $\phi(\lambda)$ is the quantum yield of the photolysis reaction. The radiative flux employed in the experiment has been previously calculated (see experimental section), and since visible light is highly reflected by our Si substrate, we have considered a total flux for wavelengths below 400 nm of 2 x 0.095 W cm^{-2} = 0.19 W cm^{-2}. Please note that the determination of the radiative flux in our experiment is affected by several uncertainties.

In order to estimate the absorption cross section of the ice mixtures, we have recorded the UV-Vis spectra of different concentrations of NH_4IO_3 solutions to calculate the molar absorptivity of this salt, which could be also expressed in absorption cross section units (the details are also given in section 5 in the supplementary information). Due to the low absorption values beyond 290 nm in the UV-Vis spectra recorded, it was necessary to extrapolate the calculated cross section values at longer wavelengths (the details are given in the supplementary information). Fig. 6 depicts the absorption cross section obtained from 200 to 400 nm, which shows a maximum value at 200 nm (2.52 x 10^{-17} cm^2 $molec^{-1}$), and a rapid decrease of around 1000 times at 300 nm (tabulated values are included in Table S3 in supplementary material).

These results are similar to those obtained for other iodate solutions (see UV-Vis spectra in Fig. 2) and, in all cases, nearly null absorptions were recorded above 300 nm, which is also in agreement with those of Saunders *et al*, (Saunders et al., 2012) and Awtrey and Connick, (Awtrey and Connick, 1951), who found nearly null absorption above 300 nm for $NaIO_3$ salt solutions. During the review process of this work, it has appeared in the literature a new study of the absorption of the iodate solutions in the UV-Vis region (Kireev and Shnyrev, 2015). In this study, the absorption cross section of KIO_3 was measured in the range from 180 to 245 nm, showing comparable values to that obtained in our study.

However, note that according to Fig. 2, the glass window shows nearly null transmission below 250 nm (where the cross section of iodate peaks). At 300 nm, the absorption cross section is around 2 x 10^{-20} cm^2 $molec^{-1}$ (although values above 300 nm should be taken with caution because the detection limit of the UV-Vis spectrometer, see section 5 in supplementary material), which is, for example, similar to that measured for CH_3I at this wavelength (J. B. Burkholder). However, CH_3I is rapidly photo-dissociated in the atmosphere (see (Saiz-Lopez et al., 2012)), while the photo-dissociation at solar-simulated irradiation of IO_3^- solutions has not been observed. Hence, the quantum yield (ϕ) of the process at the

tropospheric relevant wavelength should be very different for both systems (for CH_3I, a $\phi = 1$ is assumed).

In order to have a realistic estimation of the wavelength range relevant for iodate photolysis, we have calculated an action spectrum entailing in the product of the IO_3^- absorption cross section and the % transmittance of the glass window and the lamp output. This spectrum is shown in supplementary section, and it shows null absorption values below 250 nm, which is in fact the blue-cut-off of the glass window, registering a maximum around 290 nm, and a continued decrease of ca. 1000 times at 400 nm. At this large wavelength, the cross section of the iodate takes very low values and in fact, this region is out of our detection limit, which is given by the low absorbance values of the salt in this range (see section 5 in supplementary information). Therefore the most likely relevant wavelength interval is assumed to be from 250 to 400 nm.

Nevertheless, we should also consider that this cross section values are obtained for liquid solutions, so they could be somehow different from frozen samples as in our case. Several studies have shown that the absorbance spectrum of a species in ice could be estimated by red-shifting the solution spectrum (e.g, Dubowski and Hoffmann (Dubowski and Hoffmann, 2000)). Moreover, simulations with methyl peroxide in frozen water predict that absorption spectra are also red-shifted at low temperatures (Epstein et al., 2012). According to these previous studies, we evaluate the red-shift of the liquid cross section values of NH_4IO_3 to obtain a more realistic value of the absorption cross section of the iodate ice mixtures, as well as the implications for the estimated photolysis quantum yield (Eq. 4). Since there is no information of the quantum yield wavelength, a constant quantum yield is assumed for the entire wavelength range. The results are summarized in Table 3. The integrated value of the cross section from 250 to 400 nm peaks for a red-shift of 50 nm, while at this red-shift we obtain the lowest quantum yield value (ca. 0.0004). The opposite is obtained when the cross section values are not red-shifted. The maximum value of the product of these two magnitudes is obtained for a red-shift of 10 nm (2.61×10^{-19} cm^2 nm). This value can then be considered as the integrated cross section of the photolysis process. For comparison purposes, the integrated cross section of the photolysis of CH_3I (considering a yield of ϕ=1) in the interval from 250 to 365 nm is 2.88×10^{-17} cm^2 nm (J. B. Burkholder) which is around 100 times larger. However, our integrated value is close to that of the integrated cross section of

O_3 in the spectral interval 410–690 nm (Chappuis band), which is ca. 6.6×10^{-20} cm^2 nm (Bogumil et al., 2001).

According to these results, the photo-reactivity of the iodate salts should be related to the low-temperature effect, and the fact that iodate solutions or salts are frozen, in agreement with the results from Spolaor *et al.*(Spolaor et al., 2013). It is well known that different photochemical reactions are greatly accelerated in frozen solution due to the concentration effect of solutes in porous cavities or channels formed in the water ice network (see e.g. Grannas *et al.* (Grannas et al., 2007;Kahan et al., 2010), and references therein). For the case of NO_3^-, it has been recently shown that the photolysis in frozen ices is considerable higher than in solutions (Marcotte et al., 2015), which is similar to our observations for iodate salts.

The increase of photolysis rates at low-temperature can either be caused by a substantial change in the absorption cross section (due to a red-shift in relation to solution) or an increase of the quantum yield of the process, or in fact by both factors at the same time. Our experiments do not allow discrimination of these factors which need to be further studied in subsequent experimental work. Instead, the integrated absorption cross-section obtained in this work should be regarded as a lower limit. The reason is mainly the limitations associated with distributing the samples homogeneously during deposition, which could generate areas free of samples on the substrate. For these cases, the irradiance received by the samples could be lower than calculated (which assume a homogeneous distribution of the sample), thereby leading to a higher calculated absorption cross section value than the one obtained in this work. Based on the dispersion of our results, we have estimated that this effect could account for an increase on this value by up to a factor of two.

In addition, due to the characteristics of our experimental setup, our results represent the photolysis of the iodate in the bulk. However, as in the case of NO_3^-, this process could be much faster in the surface (Marcotte et al., 2015). In conclusion, further experiments should be conducted to confirm the values of the absorption cross section and quantum yield, and to evaluate the influence of the interface ice/air in the process of frozen iodate salts photolysis.

3.2 Atmospheric Implications

We have incorporated the experimentally-derived absorption cross section value into an atmospheric model in order to assess the implications that this process could have in polar

atmospheric chemistry. Although high levels of reactive iodine have been measured in coastal Antarctica, the emission mechanism over ice still remains unclear. We use an atmospheric model (for details see (Saiz-Lopez et al., 2008)) of the Antarctic boundary layer to assess the potential of iodate photolysis to release reactive iodine to the polar atmosphere. The model is initialized with typical concentrations of atmospheric constituents in coastal Antarctica (Jones et al., 2008) for October. An action spectrum considering Antarctic photon flux has also been calculated (see section 5 in supplementary information), which shows approximately 6 times lower intensity than that for the laboratory experiments. The reason for such difference is the smaller Antarctic sunlight photon flux. We constrain the ice surface in the model with an average iodate concentration at the ice surface of 19 nM, as recently measured over the Weddell Sea (Atkinson et al., 2012). The model incorporates a 2-stream radiation code to compute the actinic flux at the surface for springtime Antarctic irradiation conditions (Saiz-Lopez et al., 2008), and the iodate absorption cross sections and quantum yield values estimated in this work. We assume that there is an iodine atom unity conversion of iodate into reactive gas phase following iodate photolysis. This assumption is based on previous studies on the photolysis of nitrite and nitrate on ice, which pointed that 1:1 nitrogen atom conversion from inert to reacting species was necessary to model the NO_x concentrations on the Antarctic atmosphere (Boxe and Saiz-Lopez, 2008). The model sensitivities of the photoreduction of iodate in ice for the different estimated values of absorption cross sections and quantum yields provide a range of atmospheric IO levels between 0.2-1.0 pptv. These levels of IO are lower than the highest values measured in the biologically-active Weddell Sea region. However, lower IO concentrations have also been reported in other coastal regions away from the Weddell Sea (Schönhardt et al., 2008). We would like to highlight that the IO concentration range given by the model is proportional to the integrated cross section values of the photolytic process (product of the cross section and quantum yield in the selected wavelength interval) used for iodate, and therefore larger absorption cross sections would result in larger modelled IO levels. The photolysis of iodate could then provide a source of iodine that accounts for some of the comparatively low levels observed, and, to a lesser extent, also contribute to the iodine emissions over the Weddell Sea zone. Note that the model does not consider the potential loss at the ice surface of the iodine photofragments resulting from the iodate photolysis. The model results suggest, within the uncertainties highlighted above, that the photolysis of iodate on the surface of ice can potentially constitute an abiotic pathway for the release of active iodine to the polar atmosphere. Further laboratory and field work is

needed to better assess the environmental implications of the photolysis of iodate in ice surfaces.

4 Summary and Conclusions

We have explored the photolysis of ammonium iodate salt in frozen solutions. The samples were generated by different deposition methods, and at different temperatures and water concentrations, in order to obtain samples of different morphologies. The samples were processed by simulated Solar light with an average light power of 0.19 W cm^{-2} over the wavelength range of 250 to 400 nm. In the different experiments, the similar evolution of the IR spectra confirms the photolysis of iodate salts. The photolysis rates obtained are similar for all samples, within our experimental uncertainties, indicating that in the photolytic process there is a limited influence of the morphology and structure of the water ice matrix. The bands of NH_4^+ and IO_3^- decrease during irradiation and new small bands appear. As result of these experiments, the absorption cross section of iodate in an ammonium frozen salt and the quantum yield are estimated for the first time at wavelengths relevant for tropospheric studies (σ =1,22 x 10^{-17} cm^2 nm and ϕ=0.02 from 250 to 400 nm). However, due to the experimental limitations, this value has to be considered mainly as a lower limit, and further experiments are needed to confirm it. These new data have been included in an atmospheric model of the Antarctic boundary layer to assess its potential environmental relevance. The model predicts, within uncertainties, that the photolysis of iodate in ice could yield atmospheric IO levels range between 0.2-1.0 pptv, which could be higher if we consider a larger absorption cross sections for the photolysis of iodate. According to this, we suggest that the photolysis of iodate on the surface of ice can potentially constitute a pathway for the release of active iodine to the polar atmosphere.

Acknowledgements

O. G. acknowledges financial support from Ministerio de Ciencia e Innovación, "Ramón y Cajal" program and from Ministerio de Economía y Competitividad, project "CGL2013-48415-C2-1-R". M.T.B-R and M.S. acknowledge financial support from Ministerio de Economía y Competitividad, project "CGL2013-48415-C2-2". O. G., M.T.B-R and M.S. acknowledge financial support from the Spanish crowdfunding platform PRECIPITA from

FECYT foundation. Authors acknowledge the different reviewers (specially the helpful comments of referee #4) of this manuscript which have contributed to noticeably improve this article.

References

Abad, L., Bermejo, D., Herrero, V. J., Santos, J., and Tanarro, I.: Performance of a solenoid driven pulsed molecular beam source, Review of Scientific Instruments, 66, 3826-3832, doi:http://dx.doi.org/10.1063/1.1145444, 1995.

Allan, J. D., Williams, P. I., Najera, J., Whitehead, J. D., Flynn, M. J., Taylor, J. W., Liu, D., Darbyshire, E., Carpenter, L. J., Chance, R., Andrews, S. J., Hackenberg, S. C., and McFiggans, G.: Iodine observed in new particle formation events in the Arctic atmosphere during ACCACIA, Atmos. Chem. Phys., 15, 5599-5609, 10.5194/acp-15-5599-2015, 2015.

Assmy, P., Ehn, J. K., Fernández-Méndez, M., Hop, H., Katlein, C., Sundfjord, A., Bluhm, K., Daase, M., Engel, A., Fransson, A., Granskog, M. A., Hudson, S. R., Kristiansen, S., Nicolaus, M., Peeken, I., Renner, A. H. H., Spreen, G., Tatarek, A., and Wiktor, J.: Floating Ice-Algal Aggregates below Melting Arctic Sea Ice, PLoS ONE, 8, e76599, 10.1371/journal.pone.0076599, 2013.

Atkinson, H. M., Huang, R. J., Chance, R., Roscoe, H. K., Hughes, C., Davison, B., Schönhardt, A., Mahajan, A. S., Saiz-Lopez, A., Hoffmann, T., and Liss, P. S.: Iodine emissions from the sea ice of the Weddell Sea, Atmos. Chem. Phys., 12, 11229-11244, 10.5194/acp-12-11229-2012, 2012.

Awtrey, A. D., and Connick, R. E.: The Absorption Spectra of I_2, I_3^-, I^-, IO_3^-, $S_4O_6^=$ and $S_2O_3^=$. Heat of the Reaction $I_3^- = I_2 + I$, Journal of the American Chemical Society, 73, 1842-1843, 10.1021/ja01148a504, 1951.

Baker, A. R., Thompson, D., Campos, M. L. A. M., Parry, S. J., and Jickells, T. D.: Iodine concentration and availability in atmospheric aerosol, Atmospheric Environment, 34, 4331-4336, http://dx.doi.org/10.1016/S1352-2310(00)00208-9, 2000.

Baker, A. R.: Inorganic iodine speciation in tropical Atlantic aerosol, Geophysical Research Letters, 31, n/a-n/a, 10.1029/2004gl020144, 2004.

Bogumil, K., Orphal, J., Burrows, J. P., and Flaud, J. M.: Vibrational progressions in the visible and near-ultraviolet absorption spectrum of ozone, Chemical Physics Letters, 349, 241-248, http://dx.doi.org/10.1016/S0009-2614(01)01191-5, 2001.

Boxe, C. S., and Saiz-Lopez, A.: Multiphase modeling of nitrate photochemistry in the quasi-liquid layer (QLL): implications for NO_x release from the Arctic and coastal Antarctic snowpack, Atmos. Chem. Phys., 8, 4855-4864, 10.5194/acp-8-4855-2008, 2008.

Calvert, J. G., and Lindberg, S. E.: The potential influence of iodine-containing compounds on the chemistry of the troposphere in the polar spring. II. Mercury depletion, Atmospheric Environment, 38, 5105-5116, http://dx.doi.org/10.1016/j.atmosenv.2004.05.050, 2004.

Dubowski, Y., and Hoffmann, M. R.: Photochemical transformations in ice: Implications for the fate of chemical species, Geophysical Research Letters, 27, 3321-3324, 10.1029/2000gl011701, 2000.

Epstein, S. A., Shemesh, D., Tran, V. T., Nizkorodov, S. A., and Gerber, R. B.: Absorption Spectra and Photolysis of Methyl Peroxide in Liquid and Frozen Water, The Journal of Physical Chemistry A, 116, 6068-6077, 10.1021/jp211304v, 2012.

Frieß, U., Wagner, T., Pundt, I., Pfeilsticker, K., and Platt, U.: Spectroscopic measurements of tropospheric iodine oxide at Neumayer Station, Antarctica, Geophysical Research Letters, 28, 1941-1944, 10.1029/2000gl012784, 2001.

Gálvez, O., Maté, B., Herrero, V., J. , and Escribano, R.: Ammonium and Formate Ions in Interstellar Ice Analogs, The Astrophysical Journal, 724, 539, 2010.

Gálvez, Ó., Maté, B., Martín-Llorente, B., Herrero, V. J., and Escribano, R.: Phases of Solid Methanol, The Journal of Physical Chemistry A, 113, 3321-3329, 10.1021/jp810239r, 2009.

Gilfedder, B. S., Lai, S. C., Petri, M., Biester, H., and Hoffmann, T.: Iodine speciation in rain, snow and aerosols, Atmos. Chem. Phys., 8, 6069-6084, 10.5194/acp-8-6069-2008, 2008.

Grannas, A. M., Jones, A. E., Dibb, J., Ammann, M., Anastasio, C., Beine, H. J., Bergin, M., Bottenheim, J., Boxe, C. S., Carver, G., Chen, G., Crawford, J. H., Dominé, F., Frey, M. M., Guzmán, M. I., Heard, D. E., Helmig, D., Hoffmann, M. R., Honrath, R. E., Huey, L. G., Hutterli, M., Jacobi, H. W., Klán, P., Lefer, B., McConnell, J., Plane, J., Sander, R., Savarino, J., Shepson, P. B., Simpson, W. R., Sodeau, J. R., von Glasow, R., Weller, R., Wolff, E. W., and Zhu, T.: An overview of snow photochemistry: evidence, mechanisms and impacts, Atmos. Chem. Phys., 7, 4329-4373, 10.5194/acp-7-4329-2007, 2007.

J. B. Burkholder, S. P. S., J. Abbatt, J. R. Barker, R. E. Huie, C. E. Kolb, M. J. Kurylo, V. L. Orkin, D. M. Wilmouth, and P. H. Wine: Chemical Kinetics and Photochemical Data for Use in Atmospheric Studies, Evaluation No. 18, JPL Publication 15-10, Jet Propulsion Laboratory, Pasadena, 2015

Jones, A. E., Wolff, E. W., Salmon, R. A., Bauguitte, S. J. B., Roscoe, H. K., Anderson, P. S., Ames, D., Clemitshaw, K. C., Fleming, Z. L., Bloss, W. J., Heard, D. E., Lee, J. D., Read, K. A., Hamer, P., Shallcross, D. E., Jackson, A. V., Walker, S. L., Lewis, A. C., Mills, G. P., Plane, J. M. C., Saiz-Lopez, A., Sturges, W. T., and Worton, D. R.: Chemistry of the Antarctic Boundary Layer and the Interface with Snow: an overview of the CHABLIS campaign, Atmos. Chem. Phys., 8, 3789-3803, 10.5194/acp-8-3789-2008, 2008.

Kahan, T. F., Kwamena, N. O. A., and Donaldson, D. J.: Different photolysis kinetics at the surface of frozen freshwater vs. frozen salt solutions, Atmos. Chem. Phys., 10, 10917-10922, 10.5194/acp-10-10917-2010, 2010.

Kim, K., Yabushita, A., Okumura, M., Saiz-Lopez, A., Cuevas, C. A., Blaszczak-Boxe, C. S., Min, D. W., Yoon, H.-I., and Choi, W.: Production of molecular iodine and triiodide in the frozen solution of iodide: implication for polar atmosphere, Environmental Science & Technology, 10.1021/acs.est.5b05148, 2016.

Kireev, S. V., and Shnyrev, S. L.: Study of molecular iodine, iodate ions, iodide ions, and triiodide ions solutions absorption in the, Laser Physics, 25, 075602, 2015.

Klaning, U. K., Sehested, K., and Wolff, T.: Laser flash photolysis and pulse radiolysis of iodate and periodate in aqueous solution. Properties of iodine(VI), Journal of the Chemical Society, Faraday Transactions 1: Physical Chemistry in Condensed Phases, 77, 1707-1718, 10.1039/f19817701707, 1981.

Laniewski, K., Borén, H., and Grimvall, A.: Fractionation of halogenated organic matter present in rain and snow, Chemosphere, 38, 393-409, http://dx.doi.org/10.1016/S0045-6535(98)00181-7, 1999.

Maier, G., and Bothur, A.: Matrix-Isolation of Iodine Superoxide and Iodine Dioxide, Chemische Berichte, 130, 179-181, 10.1002/cber.19971300207, 1997.

Marcotte, G., Marchand, P., Pronovost, S., Ayotte, P., Laffon, C., and Parent, P.: Surface-Enhanced Nitrate Photolysis on Ice, The Journal of Physical Chemistry A, 119, 1996-2005, 10.1021/jp511173w, 2015.

Mastrapa, R. M., Sandford, R. M., Roush, T. L., Cruikshank, D. P., and Dalle Ore, C. M.: Optical Constants of Amorphous and Crystalline H2O-ice: 2.5-22 μm (4000-455 cm–1) Optical Constants of H2O-ice, The Astrophysical Journal, 701, 1347, 2009.

Mate, B., Rodriguez-Lazcano, Y., and Herrero, V. J.: Morphology and crystallization kinetics of compact (HGW) and porous (ASW) amorphous water ice, Physical Chemistry Chemical Physics, 14, 10595-10602, 10.1039/c2cp41597f, 2012.

Mate, B., Tanarro, I., Moreno, M. A., Jimenez-Redondo, M., Escribano, R., and Herrero, V. J.: Stability of carbonaceous dust analogues and glycine under UV irradiation and electron bombardment, Faraday Discussions, 168, 267-285, 10.1039/c3fd00132f, 2014.

Maté, B., Gálvez, O., Herrero, V. J., Fernández-Torre, D., Moreno, M. A., and Escribano, R.: Water-Ammonium ICES and the Elusive 6.85 μm Band, The Astrophysical Journal Letters, 703, L178, 2009.

Mayer, E.: New method for vitrifying water and other liquids by rapid cooling of their aerosols, Journal of Applied Physics, 58, 663-667, doi:http://dx.doi.org/10.1063/1.336179, 1985.

McAlpine, R. K.: The Reaction of Dilute Iodine and Ammonia Solutions, Journal of the American Chemical Society, 74, 725-727, 10.1021/ja01123a041, 1952.

Mezyk, S. P., and Elliot, A. J.: Pulse radiolysis of lodate in aqueous solution, Journal of the Chemical Society, Faraday Transactions, 90, 831-836, 10.1039/ft9949000831, 1994.

Ocampo, J., and Klinger, J.: Adsorption of N2 and CO2 on ice, Journal of Colloid and Interface Science, 86, 377-383, http://dx.doi.org/10.1016/0021-9797(82)90083-2, 1982.

Pechtl, S., Lovejoy, E. R., Burkholder, J. B., and von Glasow, R.: Modeling the possible role of iodine oxides in atmospheric new particle formation, Atmos. Chem. Phys., 6, 505-523, 10.5194/acp-6-505-2006, 2006.

Read, K. A., Mahajan, A. S., Carpenter, L. J., Evans, M. J., Faria, B. V. E., Heard, D. E., Hopkins, J. R., Lee, J. D., Moller, S. J., Lewis, A. C., Mendes, L., McQuaid, J. B., Oetjen, H., Saiz-Lopez, A., Pilling, M. J., and Plane, J. M. C.: Extensive halogen-mediated ozone destruction over the tropical Atlantic Ocean, Nature, 453, 1232-1235, http://www.nature.com/nature/journal/v453/n7199/suppinfo/nature07035_S1.html, 2008.

Roscoe, H. K., Jones, A. E., Brough, N., Weller, R., Saiz-Lopez, A., Mahajan, A. S., Schoenhardt, A., Burrows, J. P., and Fleming, Z. L.: Particles and iodine compounds in coastal Antarctica, Journal of Geophysical Research: Atmospheres, 120, 7144-7156, 10.1002/2015jd023301, 2015.

Saiz-Lopez, A., Chance, K., Liu, X., Kurosu, T. P., and Sander, S. P.: First observations of iodine oxide from space, Geophysical Research Letters, 34, n/a-n/a, 10.1029/2007gl030111, 2007a.

Saiz-Lopez, A., Mahajan, A. S., Salmon, R. A., Bauguitte, S. J.-B., Jones, A. E., Roscoe, H. K., and Plane, J. M. C.: Boundary Layer Halogens in Coastal Antarctica, Science, 317, 348-351, 10.1126/science.1141408, 2007b.

Saiz-Lopez, A., Plane, J. M. C., Mahajan, A. S., Anderson, P. S., Bauguitte, S. J. B., Jones, A. E., Roscoe, H. K., Salmon, R. A., Bloss, W. J., Lee, J. D., and Heard, D. E.: On the vertical distribution of boundary layer halogens over coastal Antarctica: implications for O3, HOx, NOx and the Hg lifetime, Atmos. Chem. Phys., 8, 887-900, 10.5194/acp-8-887-2008, 2008.

Saiz-Lopez, A., Plane, J. M. C., Baker, A. R., Carpenter, L. J., von Glasow, R., Gómez Martín, J. C., McFiggans, G., and Saunders, R. W.: Atmospheric Chemistry of Iodine, Chemical Reviews, 112, 1773-1804, 10.1021/cr200029u, 2012.

Saiz-Lopez, A., Blaszczak-Boxe, C. S., and Carpenter, L. J.: A mechanism for biologically-induced iodine emissions from sea-ice, Atmos. Chem. Phys. , 15, 9731-9746, 10.5194/acp-15-9731-2015, 2015.

Saunders, R. W., Kumar, R., MacDonald, S. M., and Plane, J. M. C.: Insights into the Photochemical Transformation of Iodine in Aqueous Systems: Humic Acid Photosensitized Reduction of Iodate, Environmental Science & Technology, 46, 11854-11861, 10.1021/es3030935, 2012.

Schönhardt, A., Richter, A., Wittrock, F., Kirk, H., Oetjen, H., Roscoe, H. K., and Burrows, J. P.: Observations of iodine monoxide columns from satellite, Atmos. Chem. Phys., 8, 637-653, 10.5194/acp-8-637-2008, 2008.

Schutte, W. A., and Khanna, R. K.: Origin of the 6.85 micron band near young stellar objects: The ammonium ion (NH4+) revisited, A&A, 398, 1049-1062, 2003.

Spolaor, A., Vallelonga, P., Plane, J. M. C., Kehrwald, N., Gabrieli, J., Varin, C., Turetta, C., Cozzi, G., Kumar, R., Boutron, C., and Barbante, C.: Halogen species record Antarctic sea ice extent over glacial–interglacial periods, Atmos. Chem. Phys., 13, 6623-6635, 10.5194/acp-13-6623-2013, 2013.

Table 1. Positions (in cm^{-1}) and assignment of the mid-IR spectra bands of the NH_4IO_3/H_2O ice mixtures shown in Fig. 3.

Experiment	**ν_1,ν_3 (IO_3^-)**	**ν_4 (NH_4^+)**	**$2\nu_1,\nu_3$ (IO_3^-)?**	**$2\nu_4,\nu_2+\nu_4,\nu_3$ (NH_4^+)**
6:1 NH_4IO_3/ H_2O 200 K	742, 792^{sh}	1428, 1451^{sh}	1683	2839, 3020, 3165
8:1 NH_4IO_3/ H_2O 100 K	738, 772^{sh}, 792^{sh}	1432, 1456^{sh}	1683	2839, 3020, 3154
4:1 H_2O/NH_4IO_3 100 K HQ	745, 769^{sh}, 794^{sh}	1432, 1456^{sh}	1683	2839, 3020, 3154^{sh}
2.:1 H_2O/NH_4IO_3 100 K Vap	749, 792^{sh}	1432, 1456^{sh}	1683	2839, 3020, 3154^{sh}

^{sh} Shoulder

Table 2. Slopes obtained in the linear regression fit of the representation of natural logarithm of the integrated intensities (in arbitrary units) of the ν_3 of IO_3^- at different time of irradiation divided by that at t=0 vs the equivalent calculation for the ν_4 band of NH_4^+ for all samples of ammonium iodate at low water proportion (see text for details).

T Irrad (K)	Slope	IO_3^-/H_2O ratio
100	0,693	8 : 1
140	0,681	1 : 1
150	0,769	5 : 1
150	0,667	4 : 1
150	0,724	5 : 1
180	0,785	3 : 1
200	0,693	5 : 1
200	0,848	8 : 1
200	0,750	6 : 1
200	0,679	1 : 3
200	0,660	3 : 1
200	0,753	6 : 1
200	0,749	6 : 1
200	0,660	8 : 1
200	0,822	8 : 1
253	0,967	2 : 1
298	1,061	15 : 1

Table 3. Quantum Yield estimation for the photolysis process studied as variation of the red-shift of the cross section (from 250 to 400 nm) obtained for the ammonium iodate solution.

nm red-shifted	Integrated Cross Section	Quantum Yield	Integrated (Cross Section x Q. Yield)
0	$1{,}224 \times 10^{-17}$	0,0200	$2{,}443 \times 10^{-19}$
10	$3{,}018 \times 10^{-17}$	0,00866	$2{,}615 \times 10^{-19}$
20	$6{,}814 \times 10^{-17}$	0,00368	$2{,}507 \times 10^{-19}$
30	$1{,}356 \times 10^{-16}$	0,00164	$2{,}227 \times 10^{-19}$
40	$2{,}587 \times 10^{-16}$	0,000783	$2{,}024 \times 10^{-19}$
50	$4{,}671 \times 10^{-16}$	0,000391	$1{,}825 \times 10^{-19}$

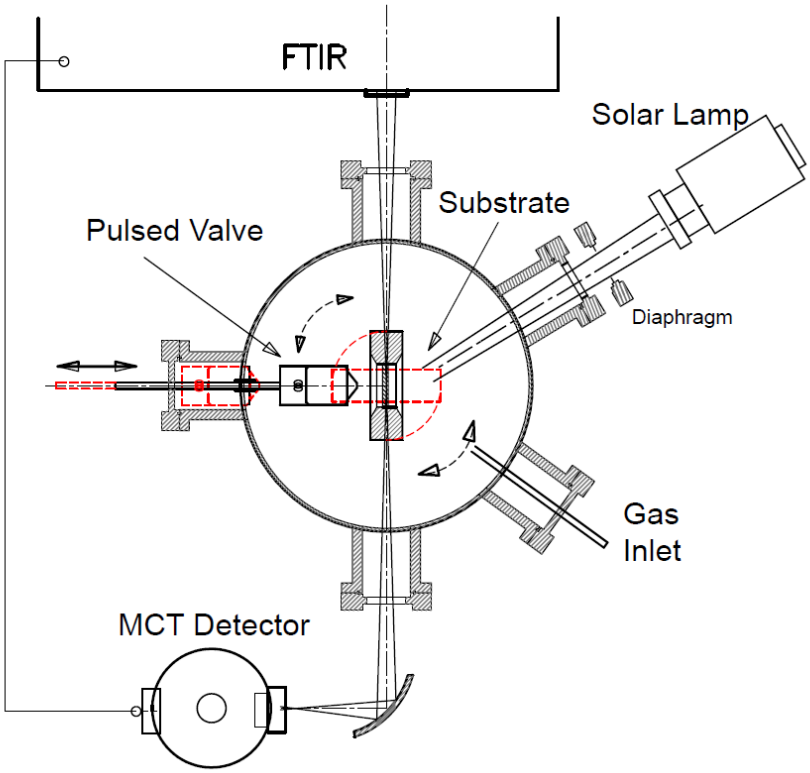

Figure 1. Schematic view of the experimental setup.

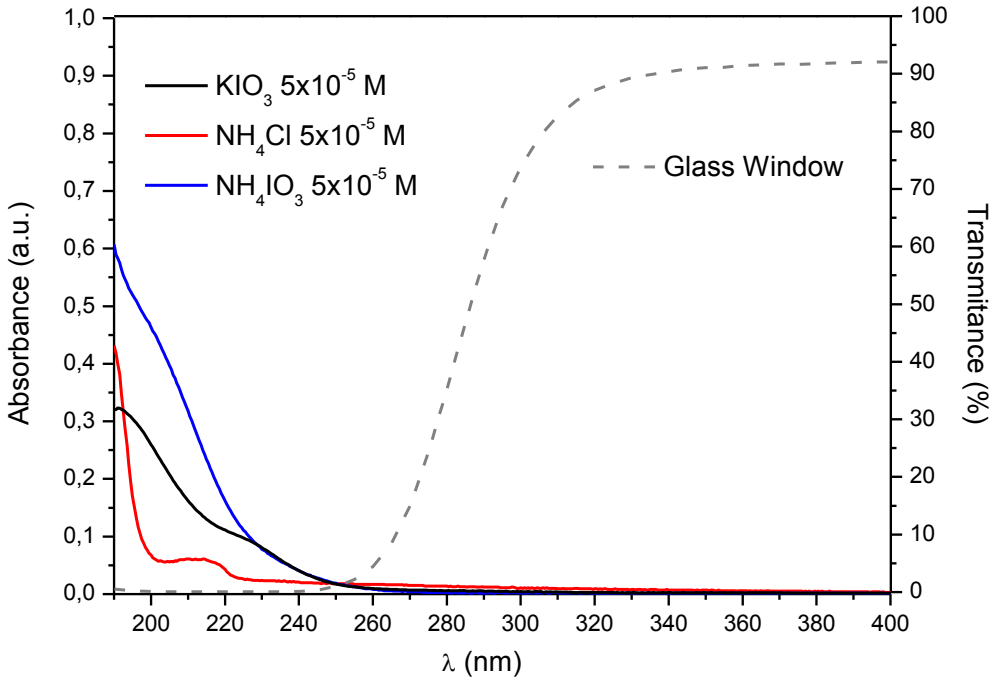

1

2 **Figure 2**. UV-Vis absorption spectra from 190 to 400 nm for KIO_3, NH_4Cl and NH_4IO_3
3 aqueous solutions (in absorbance unit) and the glass window present during irradiation (in %
4 transmittance).

5

6

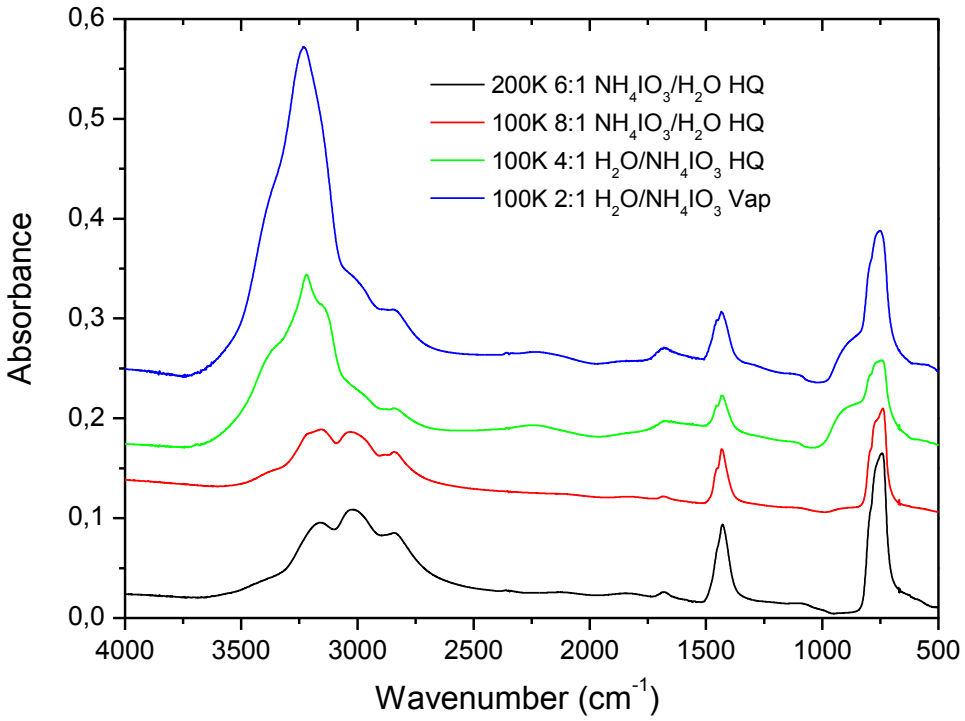

Figure 3. Mid-IR transmission spectra of pure NH_4IO_3 and H_2O/NH_4IO_3 ice mixtures generated at different temperatures.

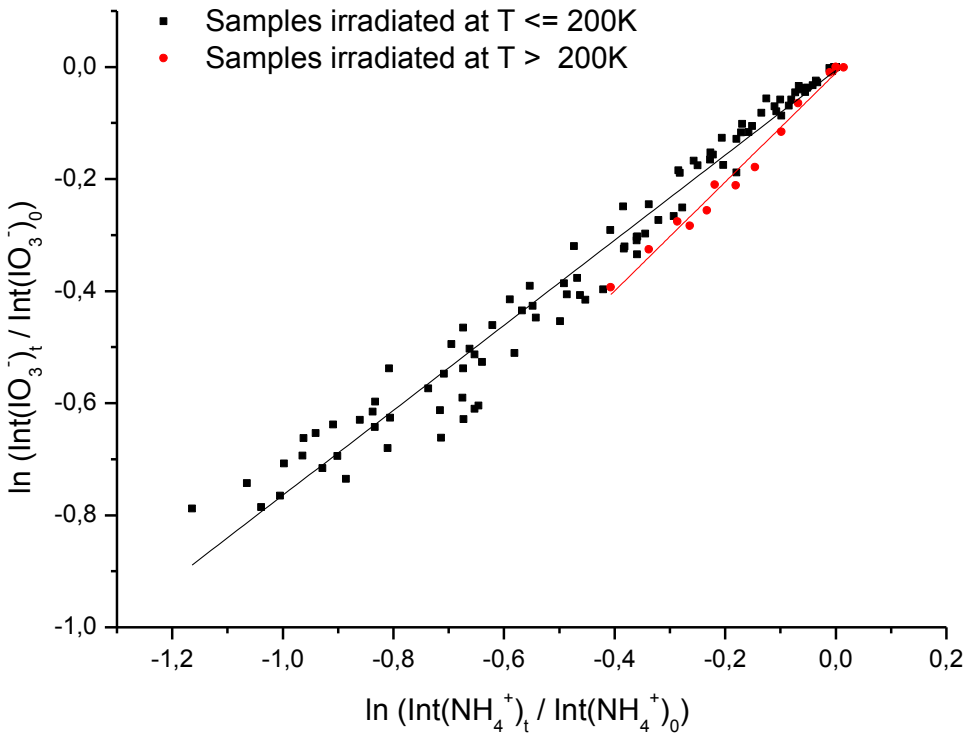

Figure 4. Natural logarithm of the integrated intensities (in arbitrary units) of the ν_3 of IO_3^- at different time of irradiation divided by that at t=0 versus the equivalent magnitude for ν_4 band of NH_4^+ for all samples of ammonium iodate shown in Table 2. Samples irradiated at T ≤ 200 K and T > 200 K are shown in black and red respectively.

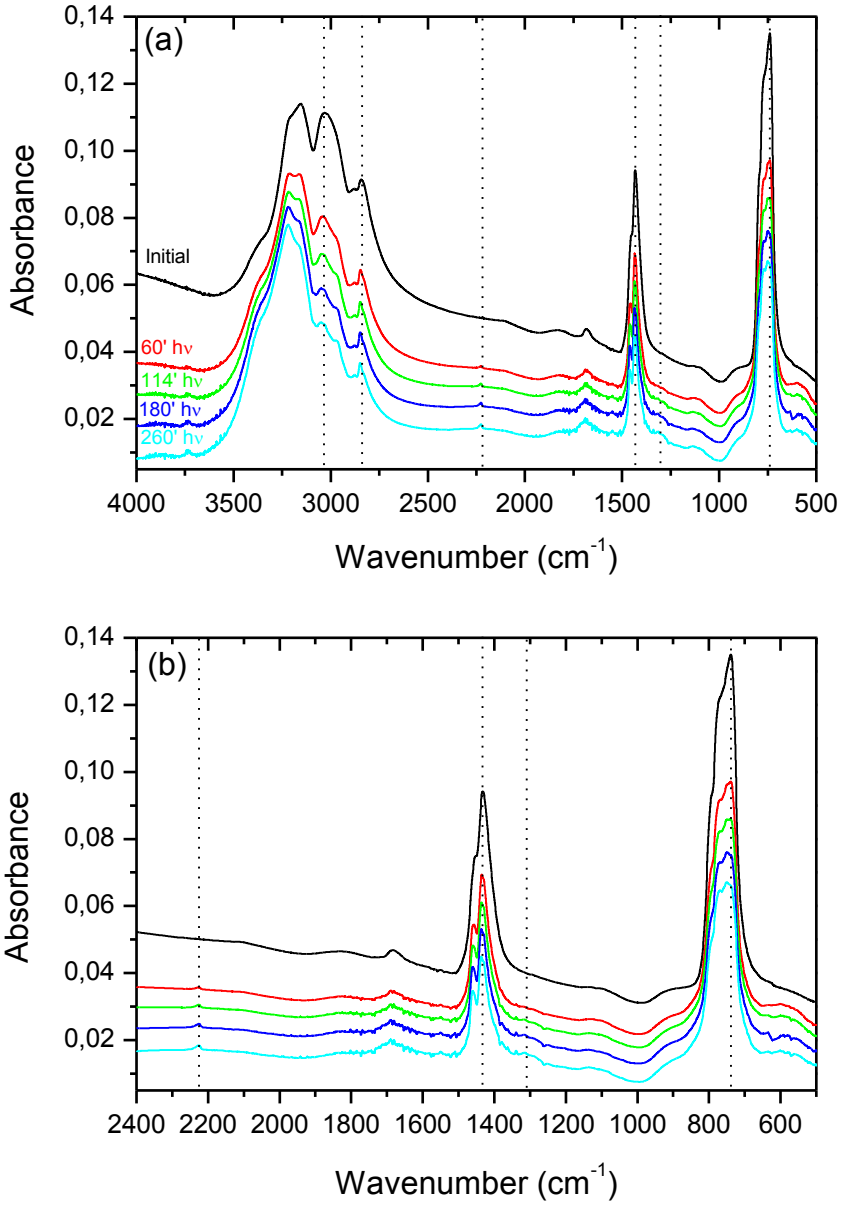

Figure 5. Evolution of the mid-IR transmission spectra of a pure NH_4IO_3 deposited at 100 K during photolysis at that temperature: Zero time, 60, 114, 180 and 260 min of photolysis in black, red, green, dark and light blue, respectively. The upper panel shows the whole IR spectra between 4000 and 500 cm^{-1}, the bottom panel is a zoom in the range 2400-600 cm^{-1}. Dotted lines indicate bands that undergo clear changes during the photolysis.

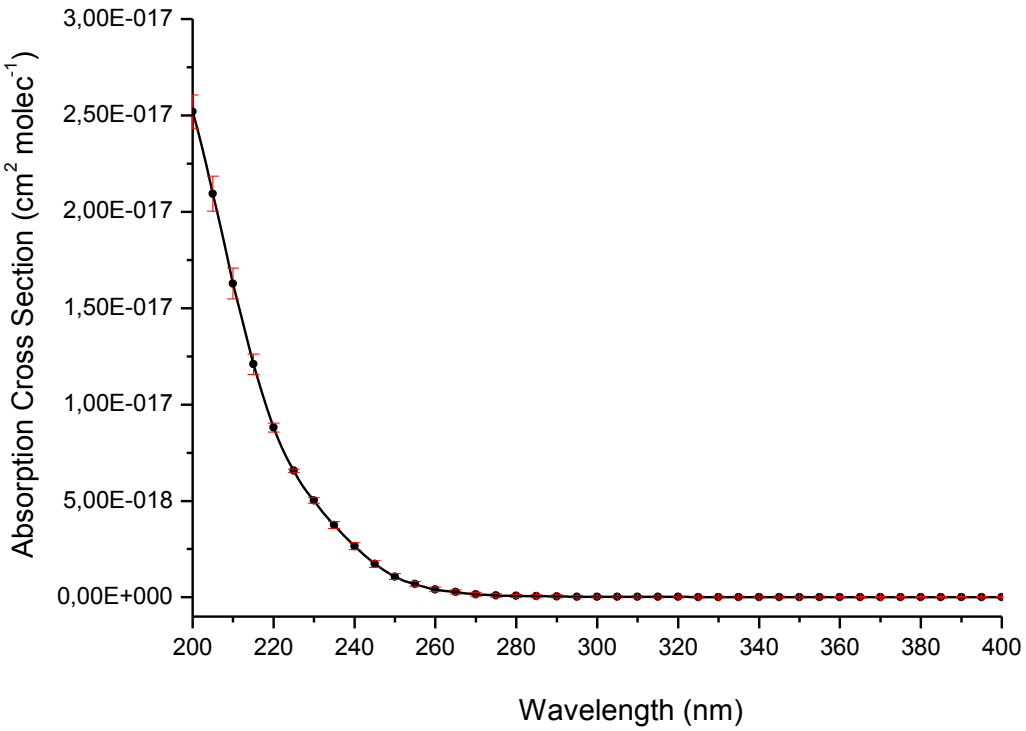

Figure 6. Absorption cross section of the ammonium iodate solution (bar errors in red).